

Li- and Mg-doping into icosahedral boron crystals, α - and β -rhombohedral boron, targeting high-temperature superconductivity: structure and electronic states

Kohei Soga,^{a,*} Atsushi Oguri,^{a,1} Satoshi Araake,^a Masami Terauchi,^b
Akihiko Fujiwara,^c and Kaoru Kimura^a

^aDepartment of Advanced Materials Science, Graduate School of Frontier Sciences, The University of Tokyo, Kiban Bldg. 50215A5, 5-1-5 Kashiwanoha, Kashiwa, Chiba 277-8561, Japan

^bInstitute of Multidisciplinary Research for Advanced Materials, Tohoku University, 2-1-1 Katahira, Aoba-ku, Sendai 980-8577, Japan

^cSchool of Materials Science, Japan Advanced Institute of Science and Technology, 1-1 Asahidai, Tatsunokuchi, Ishikawa 923-1292, Japan

Received 9 January 2003; accepted 19 May 2003

Abstract

The possibility of high T_C superconductivity is suggested for lithium- and magnesium-doped icosahedral boron crystals, α - and β -rhombohedral boron. The doping of these elements was attempted by a vapor diffusion processing. Both lithium and magnesium are hardly doped into the α -rhombohedral boron, although small amounts of metallic parts are found in the sample. In only one Li-doped sample, the metallic part contained 0.02 vol% of the superconductive phase ($T_C \sim 36$ K). Magnesium was successfully doped into β -rhombohedral boron homogeneously up to 4 at% ($\text{Mg}_{4.1}\text{B}_{105}$), although considerable amount of impurity silicon was introduced together with magnesium. The structures of the doped samples were analyzed assuming co-doping of magnesium and silicon. The relation between the site occupancies of the dopants and the lattice expansion is discussed. The estimation of the density of states near the Fermi energy by EELS and magnetic susceptibility measurements suggested a metal transition of the β -rhombohedral boron by the doping of magnesium and silicon. The relation between the metal transition and the intrinsic acceptor level is also discussed.

© 2003 Elsevier Inc. All rights reserved.

Keywords: Superconductivity; Lithium; Magnesium; Boron; Cluster solids

1. Introduction

Elemental boron (B), such as α - and β -rhombohedral B (α -B, β -B) or amorphous B (a-B), have a framework crystal structure built up from B_{12} icosahedral clusters. These structures have considerably large interstitial doping sites, where they can accept several and up to 20 at% of other elements without destructing the original structure in the undoped form [1–7]. We have reported that the doping of metallic elements into these sites reveals interesting variety of the change in physical properties of β -B [8–11] and a-B [12, 13]. For example, vanadium (V) only occupies the A_1 site and lithium (Li)

occupies only the D and E sites among the major dope sites. A V-doping causes hybridization between B and V resulting in metal transition with only a few at% doping, while rigid band scheme seems to hold for Li-doping up to the solubility limit of Li into β -B, $\text{Li}_8\text{B}_{105}$. The intrinsic acceptor level (IAL) of β -B can accept at most 8 electrons. Thus, the Li-doping into β -B up to the solubility limit only causes the filling up of the IAL and the Fermi energy does not reach the conduction band.

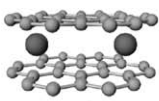
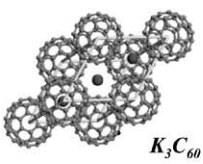
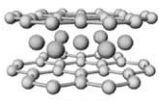
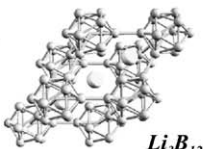
Another remarkable character of icosahedral cluster solids is possibility of relatively higher density of states (DOS) near the Fermi energy due to the high symmetry of the cluster unit. The high symmetry of the B_{12} cluster, icosahedral symmetry, gives rise to high degeneracy of the electronic states, which accordingly results in the high DOS. If one can adjust the Fermi energy to the energy with the high DOS, there is a possibility of higher critical temperature (T_C) of superconductivity for the

*Corresponding author. Fax: +81-4-7136-3759.

E-mail address: mail@ksoga.com (K. Soga).

¹Present address: The Furukawa Electric Co., Ltd., 6 Yawata-kaigandori, Ichihara, Chiba 290-8555, Japan.

Table 1
Comparison between layered and cluster solids based on carbon and boron

Major component	Layered solids	Cluster solids		
Carbon	KC₈ $N(E_F)^a \sim 14$ states/eV nm ³ $T_C \sim 0.1$ K	 KC₈	K₃C₆₀ $N(E_F)^a \sim 25$ states/eV nm ³ $T_C \sim 20$ K	 K₃C₆₀
Boron	MgB₂ $N(E_F)^a \sim 24$ states/eV nm ³ $T_C \sim 40$ K	 MgB₂	Li_xB₁₂ $N(E_F)^a \sim 39$ states/eV nm ³	 Li_xB₁₂

^aThe values of $N(E_F)$ were calculated referring [16, 17, 20, 15] for KC₈, K₃C₆₀, MgB₂ and Li_xB₁₂, respectively.

icosahedral cluster solid. Gunji et al. [14,15] performed a first-principle study on Li-doped α -B (Li_xB₁₂) and predicted the superconductivity. Table 1 shows the comparison of the solids with layered structures and the cluster solids. In the case of carbon (C) rich solids, the KC₈ has a layered structure [16] and T_C is 0.1 K. On the other hand, K₃C₆₀ is a cluster solid consisting of C₆₀ clusters, which have the same icosahedral symmetry as B₁₂ clusters. The icosahedral symmetry results in high DOS because of its isotropy. Accordingly, a doped fullerene solid K₃C₆₀ has much higher DOS at the Fermi energy ($N(E_F)$) and T_C [17,18] than those for the layered KC₈. For the same reason, B-rich icosahedral cluster solids should have higher T_C than the B-rich solids with layered structure. Typical layered structure B-rich solids are diborides, which have the same honeycomb layers as KC₈. MgB₂ is one of diborides and has T_C of 39 K [19]. The reasons for the much higher T_C of MgB₂ than that of KC₈ with the similar structure is mainly the higher frequency phonon coupled with conduction electrons because E_F is located in the π - and σ -bands for KC₈ and MgB₂, respectively [20,21]. The same situation may apply for the case of cluster solids. Furthermore, the observation of bipolaron hopping conduction for B₄C, which consists of the B₁₂, also supports the strong electron–lattice interaction in the B-rich cluster solids [22]. Thus, one can expect much higher T_C for the B-rich cluster solids than the layered MgB₂. According to the BCS theory, the T_C is roughly expressed as

$$T_C \propto \omega \exp\left(-\frac{1}{VN(E_F)}\right), \quad (1)$$

where ω is the phonon frequency and V is the electron–phonon coupling constant. As described above, all of the three factors, ω , V and $N(E_F)$, of B-rich icosahedral cluster solids act desirable to accomplish a high T_C .

We reported a study on Li-doping on β -B [8]. As shortly described above, the Li-doping only filled up the IAL and we could not even observe a metal transition. Magnesium (Mg) is an element, which has an atomic radius similar to that of Li and may donate two electrons to the β -B since a stable Mg ion is a divalent ion. Thus, we can expect to push the Fermi energy above the IAL into the conduction band with about half the number of Mg than the case of Li. In the present work, we report the study on Li-doping to α -B and Mg-doping to α - and β -B. The structure and electronic states, together with magnetic and superconductive properties of the doped B will be discussed.

2. Experimental

The α -B was prepared by crystallizing a-B powder with 3 N purity by a method similar to that reported in the literature [23,24]. The a-B powder placed in a tantalum tube with 3 N purity was sealed in a quartz tube with argon gas at 18.7 kPa pressure. The tube was heated up to 1200°C and maintained for 10 h. The formation of the α -B was confirmed by an X-ray diffraction (XRD). As for the β -B, commercial 2 and 5 N powders were used.

Li or Mg was doped in α - or β -B by a vapor diffusion processing (VDP), which is essentially the same way used for the Li-doping into β -B [8]. α - or β -B powder was placed on one side and bits of Li and Mg with 3 N purity on the other side of a tantalum or boron nitride reaction tube. The reaction tube was sealed in an evacuated quartz tube doubly and singly for Li and Mg, respectively, and heated up and kept at different temperatures between 700°C and 1300°C for a desired time.

The samples are examined by an XRD with CuK α radiation in the 2θ range from 10° to 80°. The lattice

constants were determined by analyzing the peaks between 37° and 57° , calibrating the angle using silicon powder mixed with the samples in this measurement. The XRD patterns of doped and undoped β -B were analyzed by the Rietveld method to determine the site occupancies of the dopants. A program RIETAN2000 was used for the Rietveld refinement [25].

Electron energy-loss spectroscopy (EELS) was applied for the samples to obtain information of the DOS of the conduction band. A specimen-cooling holder with liquid nitrogen was used and the recording time was set as short as 90 s for the Li-doped sample to avoid the evaporation of Li from the doped sample by electron beam irradiation. Mg-doped sample was stable under the electron beam irradiation. The details of the EELS measurement were described in other papers [26,27].

The magnetic susceptibility of the samples was measured by using a superconducting quantum interference device (SQUID) magnetometer. The sample was first cooled to 2 K under a zero field and the signal was recorded under a field during warming (zero-field cooled, ZFC). Then the signal was recorded under the same field during the cooling down to 2 K (field-cooled, FC). The applied strength of the magnetic field was 10 Oe for the examination of superconductivity and 10,000–50,000 Oe for the observation of other magnetic properties.

3. Results and discussion

3.1. Li- and Mg-doping on α -rhombohedral boron

Doping of Li and Mg into α -B was attempted by the VDP under the conditions shown in Fig. 1. The temperature was set at 900–1220°C for Li-doping and at 700–1220°C for Mg-doping. The samples were kept at these temperatures for 2–70 h. Fig. 2(a) shows the typical XRD patterns of the samples denoted as Li- α -1 and Mg- α -1 in Fig. 1 together with that of undoped α -B. The XRD patterns are almost the same for all samples. None of the peaks of stoichiometric lithium or magnesium borides was found, although the small peaks of impurities as β -B, B_6O and TaB_2 were detected beside the peaks of α -B. The origin of TaB_2 is the contamination from reaction of the boron powder with the Ta tube. The identity of the XRD patterns among the samples means that Li and Mg were not doped in whole sample of α -B.

The samples showed mostly red color of α -B. Only some parts of samples showed metallic glittering. We picked out the glittering particles and examined under a TEM equipped with an EELS measurement system. The patterns of Bragg spots of electron diffraction from the particles were almost the same as that of undoped α -B. The results of the EELS measurement are shown in

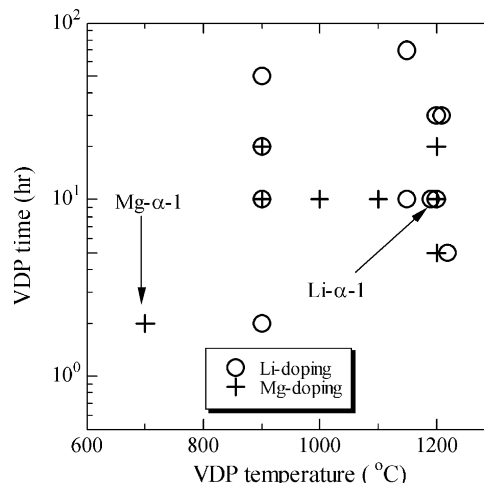


Fig. 1. VDP conditions for Li- and Mg-doping into α -B. The conditions indicated by arrows are those for the samples used for the EELS measurement.

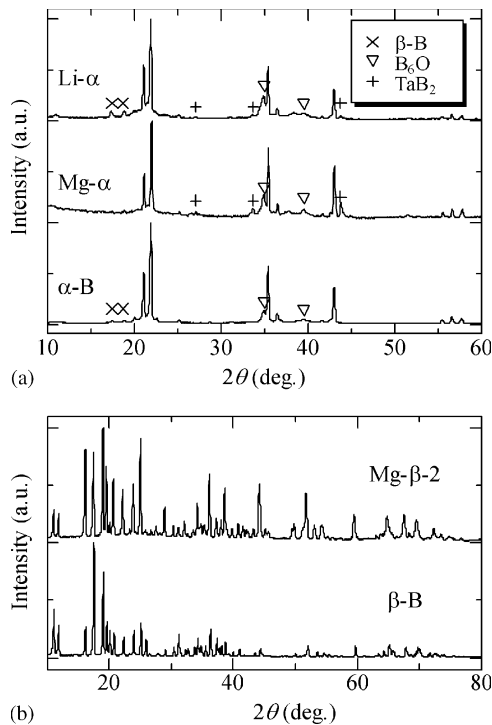


Fig. 2. XRD patterns of (a) undoped, Li- and Mg-doped α -B and (b) undoped and Mg-doped β -B.

Fig. 3(a) [26] together with the DOS in Fig. 3(b) of undoped α -B obtained by using first-principle calculation, which was quoted from the paper by Gunji et al. [15]. The spectrum of pure α -B agreed well with the calculated DOS of the conduction band. By the VDP of Li and Mg, the main peaks at 191 eV shifted to the lower energy. The stepwise increase of the signal indicated by an arrow in Fig. 3(a) is considered to be the Fermi edge. This chemical shift and the appearance of the Fermi

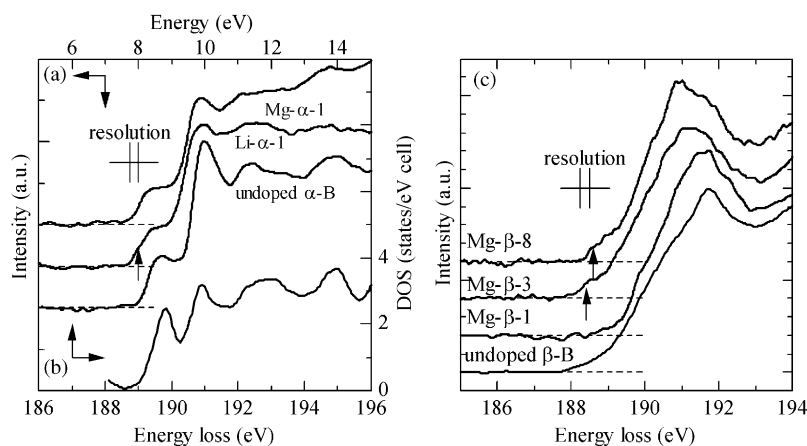


Fig. 3. EELS spectra of (a) undoped, Li- and Mg-doped α -B (Li- α -1, Mg- α -1) and (c) undoped and Mg-doped β -B (Mg- β -1, 3 and 8) [26]. The arrows indicate the stepwise increase of the signal described in the text. (b) shows the results of first-principle calculation by Gunji et al. [15].

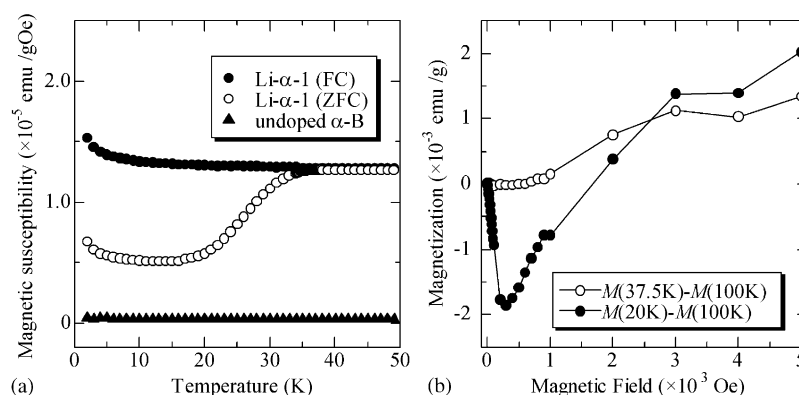


Fig. 4. Magnetic susceptibility of undoped and Li-doped α -B (Li- α -1). (a) Dependence on temperature under zero-field cool (ZFC) and field cool (FC) and (b) dependence on the strength of the applied magnetic field. The values at 100 K is subtracted from those at 20 and 37.5 K to eliminated the effects of ferromagnetic impurities.

edge mean the increase of the electrons in the conduction band. More precise reading of the EELS data is described in Ref. [26].

The glittering and the chemical shift of the particles suggest a metal transition of α -B due to the doping of Li and Mg, although the change of the XRD pattern was under detection since the doping was only partial. To examine the superconductivity, we performed a magnetization measurement for the samples. We could not observe superconductivity except the only one sample, Li- α -1. Fig. 4(a) shows the temperature dependence of magnetic susceptibility, χ , of undoped α -B and the sample Li- α -1 under conditions of zero-field cooling (ZFC) and field cooling (FC) at a magnetic field of 200 Oe [28]. A drop of the χ observed for the Li- α -1 under the ZFC is possibly due to the shielding effect. The positive shift of the χ for the Li- α -1 should be originated from an unknown ferromagnetic impurity. The T_C is estimated to be 36 K, which is slightly lower than $T_C = 39$ K for MgB_2 [19]. The estimated volume fraction (ratio) of the superconductive phase to the whole sample was only 0.02%. The magnetization under

varied magnetic field above and below the T_C is shown in Fig. 4(b) [28]. The magnetization at 100 K was subtracted from both of the values at 20 and 37.5 K to eliminate the temperature-independent component due to the ferromagnetic impurity. The magnetization at 20 K is negative under a weak magnetic field and approaches to the value at 37.5 K by increasing the magnetic field. This result supports that the drop of χ in Fig. 4(a) is caused by the shielding effect. The increase of the magnetization above 2×10^3 Oe is due to the temperature-dependent Curie–Weiss term and will be discussed in the later section for β -B. We should wait for the development of the synthesis method of Li- or Mg-doped α -B and not assert that the superconductive phase is Li-doped α -B since the volume fraction of the phase is too small.

3.2. Structure of Mg-doped β -rhombohedral boron

Mg was doped successfully into β -B with 2N purity by the VDP at a fixed temperature of 1200°C. The amount of the doped Mg was a few percent by the VDP

Table 2

VDP conditions, lattice constants, a_{hex} and c_{hex} and volume, V , of the hexagonal unit cell in pure and (Mg, Si) doped β -rhombohedral boron. The values are listed in order of the length of lattice constant a_{hex}

Sample name	VDP condition	a_{hex} (Å)	c_{hex} (Å)	V (Å ³)
β -B	—	10.9270 ± 0.0008	23.828 ± 0.008	2463.9 ± 0.3
Mg- β -1	1200(°C) 10(h)	10.980 ± 0.002	24.035 ± 0.004	2509.6 ± 0.7
Mg- β -2	1200(°C) 10(h)2(times)	10.9880 ± 0.0008	24.084 ± 0.002	2518.2 ± 0.3
Mg- β -3	1200(°C) 10(h)3(times)	10.998 ± 0.002	24.122 ± 0.004	2526.8 ± 0.9
Mg- β -4	1200(°C) 10(h)4(times)	11.008 ± 0.002	24.130 ± 0.003	2532.2 ± 0.5
Mg- β -5	1200(°C) 10(h)5(times)	11.0101 ± 0.0008	24.120 ± 0.002	2532.2 ± 0.3
Mg- β -6	1200(°C) 10(h)4(times)	11.011 ± 0.001	24.122 ± 0.003	2532.9 ± 0.5
Mg- β -7	1200(°C) 10(h)6(times)	11.021 ± 0.002	24.122 ± 0.003	2536.3 ± 0.6
Mg- β -8	1200(°C) 10(h)7(times)	11.039 ± 0.001	24.111 ± 0.002	2544.5 ± 0.4
Mg- β -9	1200(°C) 40(h)	10.958 ± 0.002	23.962 ± 0.003	2491.9 ± 0.8
Mg- β -10	1200(°C) 100(h)	11.060 ± 0.001	23.990 ± 0.002	2541.2 ± 0.4
Mg- β -11	1200(°C) 200(h)	11.0647 ± 0.0008	23.992 ± 0.002	2543.8 ± 0.3

for 10 h. To dope more Mg, we applied longer VDP time up to 200 h or multiple doping of 10 h up to 7 times. The VDP conditions are listed in Table 2 together with the lattice constants and volumes of the hexagonal unit cell, which are obtained by the XRD. We use the sample name listed in the table to denote a sample in the following part. The a - and c -axis expanded up to 1.26% and 0.68% by the doping, respectively. The XRD patterns of undoped β -B and Mg- β -1 as an example of doped samples are shown in Fig. 2(b). Although the shifts and intensity changes of the peaks were observed, we found that the framework of the β -B remained after Mg doping since the overall profile did not change essentially. To confirm the doping of Mg, energy dispersive spectroscopy (EDS) was performed for some of the samples. As a result, considerable amount of silicon (Si) was doped in the sample beside the Mg. The source of the Si may be the quartz tube used for the VDP because Mg is a strong reducer and quartz should be reduced to form atomic Si. Therefore, we carried out the Rietveld refinement on the XRD patterns of the Mg- β -1–11 assuming co-doping of Mg and Si.

For the Rietveld refinement of the crystal structure, we selected the doping site of Mg and Si atoms according to literature. In the following part, the notation of the site is according to those in literature [1,29,30]. We assumed the sites for Si to be the A_1 , A_2 and B1 since Vlasse et al. reported [1] that Si atoms occupy these sites in the β -B. Then we eliminated the A_2 site from the Si sites after several trials since the occupancy of Si at A_2 resulted in negative values. Recently, the dope sites of Mg have been reported to be D , E and F [29]. It is known from literature [1–4,19,22] that all of the metal atoms occupy A_1 , D , E or F sites. Also, atoms larger than aluminum do not occupy A_1 site. Therefore, we assumed D , E and F sites as the dope sites for Mg. For the simplicity of the analysis, all of the interstitial sites of B, BN with $N > 15$, were neglected. The site occupancies of Si and Mg are listed on Table 3

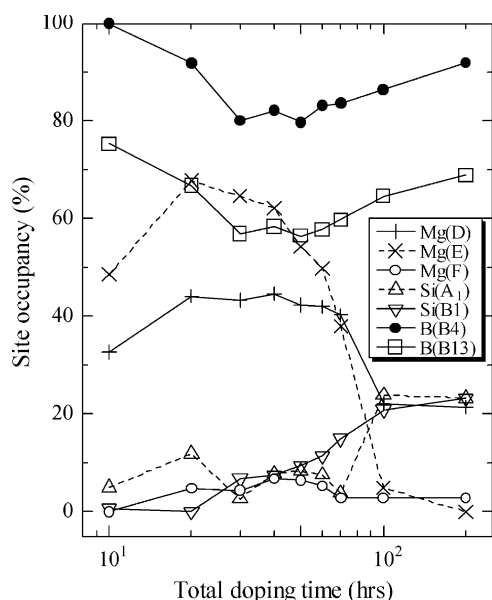
together with the R_{wp} , which is a measure of the refinement quality [4,31]. The occupancy of B at B13 is also listed, which is known to be $\sim 75\%$ for pure β -B [30]. The values of R_{wp} (9–11%) are comparable or less than those reported for LiB_{13} (11–17%) [4]. Fig. 5 shows the relation between the total doping time and site occupancies. On the first stage, the occupancies of Mg at both D and E sites increase by up to 40 h. After 40 h, the occupancy of Mg decreases and that of Si increases. The occupancies of Si at the B1 site and Mg at the E site behaved oppositely. In the same way, the behavior of the occupancies of Mg and B at B4 and B13 sites were opposite. Fig. 6 shows the schematic illustration of the above sites in β -B. The B1 sites are between A_1 and E sites. On the first stage, Mg occupies the D , E and F sites and then Si atoms take place to be doped at the A_1 or B1 site. After 40 h doping, the Si atoms ejected the Mg atoms because the doping of both Si in the B1 and Mg in the E sites may cause too much tension to the structure since the atomic radius of Si is larger than that of B. Finally, by the continuous doping of silicon up to 100 h, the E site with Mg was emptied. Referring to the discussion in the next paragraph, the reason of the decrease of Mg at the D site is not clear but the anisotropic cell expansion due to Si doping opposite to that due to Mg may cause the tension to eject the Mg from the D site. In the same way, when the occupancy of Mg at the D and F sites increased, the neighbor B atoms at B13 and B4 sites may be ejected to relax the structure. For B13 deficiency naturally occurs even for pure β -B.

In Figs. 7(a) and (b), the lattice constants and the number of doped Mg and/or Si are correlated. As seen from Fig. 7(a), the doping of both Mg and Si caused the expansion of the cell to the a -axis orientation. Also, the figure clearly shows that the ejection of Mg was mainly caused by the doping of Si at the B1 site. On the other hand, the only correlation found for the a -axis expansion was a linear correlation between the number of Mg at D site and Si at B1 site. To separate the effects of

Table 3

Reliability factor, R_{wp} , and occupancy of partially occupied site as results of Rietveld analysis on (Mg, Si) doped β -rhombohedral boron

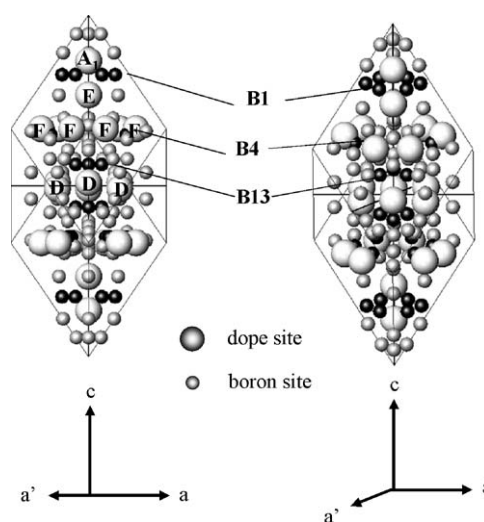
Sample name	Composition	Occupancy (%)							R_{wp} (%)
		Si (A_1)	Mg (D)	Mg (E)	Mg (F)	B (B_4)	Si (B_1)	B (B_{13})	
β -B	B_{105}	0	0	0	0	100	0	75	—
Mg- β -1	$Mg_{2.9}Si_{0.17}B_{105}$	5.0 ± 0.5	32.7 ± 0.4	48.6 ± 0.5	0	100	0.6 ± 0.3	75 ± 1	10.4
Mg- β -2	$Mg_{4.3}Si_{0.24}B_{105}$	11.9 ± 0.5	44.2 ± 0.4	67.8 ± 0.6	4.8 ± 0.7	92 ± 1	0.0	67 ± 1	9.78
Mg- β -3	$Mg_{4.2}Si_{0.87}B_{105}$	2.7 ± 0.5	43.3 ± 0.4	64.6 ± 0.6	4.4 ± 0.5	80 ± 1	6.8 ± 0.4	57 ± 1	9.33
Mg- β -4	$Mg_{4.3}Si_{1.05}B_{105}$	7.8 ± 0.5	44.6 ± 0.4	62.2 ± 0.6	6.8 ± 0.6	82 ± 1	7.5 ± 0.3	58 ± 1	9.79
Mg- β -5	$Mg_{4.0}Si_{1.30}B_{105}$	8.3 ± 0.4	42.4 ± 0.4	54.2 ± 0.6	6.4 ± 0.6	80 ± 1	9.4 ± 0.3	57 ± 1	9.12
Mg- β -6	$Mg_{4.0}Si_{1.25}B_{105}$	5.9 ± 0.5	41.5 ± 0.4	52.9 ± 0.5	7.6 ± 0.6	78 ± 1	9.4 ± 0.3	54 ± 1	9.02
Mg- β -7	$Mg_{3.8}Si_{1.52}B_{105}$	7.6 ± 0.5	42.0 ± 0.4	49.9 ± 0.6	5.3 ± 0.6	83 ± 1	11.4 ± 0.3	58 ± 1	9.36
Mg- β -8	$Mg_{3.3}Si_{1.88}B_{105}$	3.8 ± 0.5	40.3 ± 0.4	38.0 ± 0.6	2.8 ± 0.5	84 ± 1	15.0 ± 0.4	58 ± 1	8.99
Mg- β -9	$Mg_{2.2}Si_{0.46}B_{105}$	22.8 ± 0.4	17.5 ± 0.3	43.6 ± 0.5	5.0 ± 0.7	83 ± 1	0.0	68 ± 1	10.1
Mg- β -10	$Mg_{1.6}Si_{2.99}B_{105}$	23.9 ± 0.4	22.2 ± 0.3	4.9 ± 0.7	2.8 ± 0.8	86 ± 1	21.0 ± 0.3	65 ± 1	8.54
Mg- β -11	$Mg_{1.5}Si_{3.26}B_{105}$	23.3 ± 0.5	21.4 ± 0.3	0.0	2.9 ± 0.9	92 ± 1	23.3 ± 0.4	68 ± 1	9.07

Fig. 5. Dependence of site occupancy on total doping time for Mg-doped β -B.

Si- and Mg-doping, we assumed a linear correlation between the dopant contents and the lattice constants, and applied a least-squares fit to the observed lattice constants using the equations

$$\begin{aligned}
 a &= f_{Si}^a x_{Si} + f_{Mg}^a x_{Mg} + a_0, \\
 c &= f_{Si}^c x_{Si} + f_{Mg}^c x_{Mg} + c_0,
 \end{aligned} \quad (2)$$

where a , c are the lattice constants, a_0 , c_0 are lattice constants of undoped β -B, x_M is the content of dopant M in at% and $f_M^{a \text{ or } c}$ are linear coefficients obtained as fitting parameters. The results of the fitting are shown in Fig 7(c). The correlation coefficients were 0.99 for both a - and c -axis. The correspondence of the site occupancy obtained by Rietveld refinement and the lattice constants obtained from the peak positions of XRD patterns support the reliability of the results of the

Fig. 6. Schematic illustration of the dope sites in β -B (B_{105}).

Rietveld refinement. The obtained linear coefficients are $f_{Si}^a = 3.99 \times 10^{-2}$, $f_{Mg}^a = 1.00 \times 10^{-2}$, $f_{Si}^c = 2.17 \times 10^{-2}$ and $f_{Mg}^c = 6.98 \times 10^{-2} (\text{\AA}/\text{at}\%)$. These values are comparable to those obtained for single element doping from the literature, $f_{Si}^a = 3.27 \times 10^{-2}$, $f_{Si}^c = 1.09 \times 10^{-2}$ [1], $f_{Mg}^a = 0.91 \times 10^{-2}$ and $f_{Mg}^c = 7.39 \times 10^{-2} (\text{\AA}/\text{at}\%)$ [29]. The doping of Si has ~ 4 times more effect on the a -axis expansion. On the other hand, Mg-doping affected the c -axis expansion ~ 3 times more than Si-doping. Thus, we conclude that the doping of Si and Mg are effective to the expansions of the cell in a - and c -axis directions, respectively.

3.3. Electronic states and magnetic properties of Mg-doped β -rhombohedral boron

Fig. 3(c) shows the results of EELS measurements [27] on β -B, Mg- β -1, 3 and 8. A stepwise increase of the signal indicated by arrows was observed for the samples

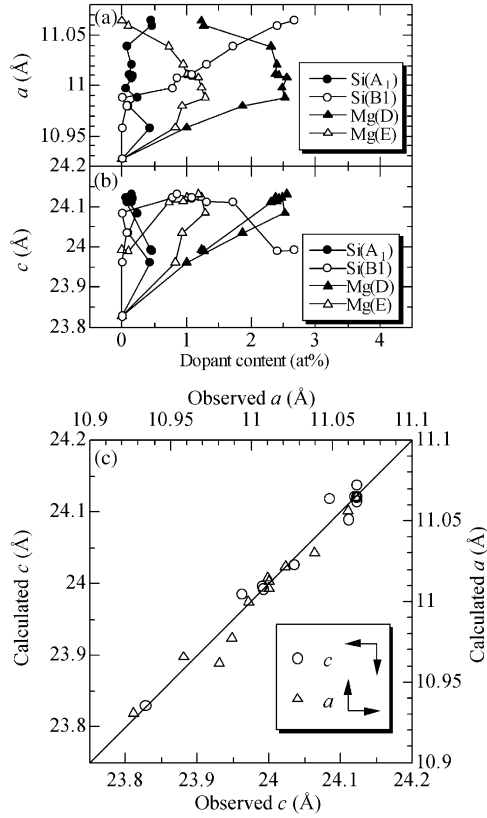


Fig. 7. Relation between dopant contents and the cell expansion of β -B in a -axis (a) and c -axis (b) direction. (c) Shows the correlation between observed lattice parameters and calculated ones by Eq. (2).

Mg- β -3 and 8 around 188.5 eV. We can take it as a discontinuous increase of the signal since the resolution of the measurement is 0.26 eV. This discontinuous increase of the signal is due to the formation of Fermi edge in the conduction band. The formation of Fermi edge suggests the possibility of metal transition of β -B by Mg-doping. More precise reading of the ELLS data is described in Ref. [27].

Temperature dependencies of magnetic susceptibility, χ , of selected samples were measured to investigate the Mg-doping effects on the electronic states. The results are shown in Fig. 8. Although no transition due to superconductivity was observed, the samples showed temperature-dependent magnetism. The χ of a substance at a temperature T can be fitted as

$$\chi = \chi_0 + \chi_{CW} = \chi_0 + \frac{C}{T - \theta_p}, \quad (3)$$

where χ_0 is a temperature-independent part. The second term is a temperature-dependent part obeying Currie–Weiss (CW) law, where θ_p is the Weiss temperature. The C is the Currie constant and described as

$$C = \frac{N \mu_B^2 p_{\text{eff}}^2}{3k_B}, \quad (4)$$

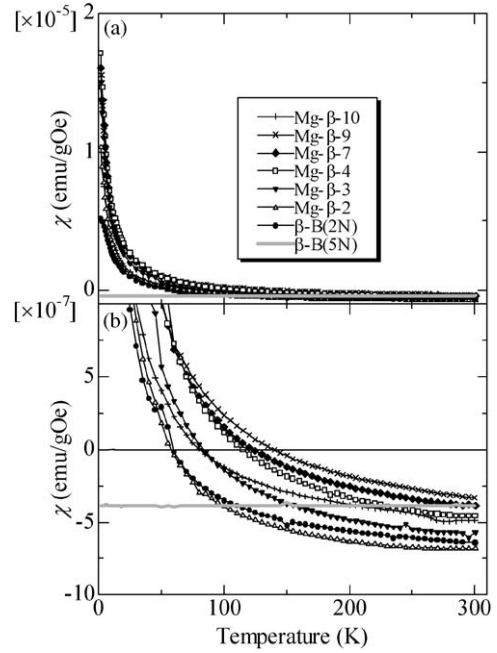


Fig. 8. Temperature dependence of magnetic susceptibility of undoped and Mg doped β -B (a), (b) is magnified plots to show the negative values at a room temperature.

where p_{eff} is the effective Bohr magneton and N is the spin density. The contribution of χ_{CW} increased by increasing the Mg content. The data in Fig. 8 was completely fit by Eq. (3) and χ_0 , C and θ_p were obtained as fitting parameters for each sample. The results are shown in Table 4. To investigate the origin of this χ_{CW} , we also measured the χ of pure β -B with 5 N purity, for which χ_{CW} was not observed as shown in Fig. 8. Thus, the Mg-doping may not be only the origin of χ_{CW} but the impurity in β -B with 2 N purity is also a possible reason of the CW component. A major impurity in 2 N β -B is 0.1 wt% of Mg, which corresponds to 0.05 at%. Therefore, it is natural to think that the origin of χ_{CW} is the Mg-doping. It is reported that the dopants at A_1 or D site forms a pair and originate an antiferromagnetism for β -B doped with manganese or iron [32,33]. In the present case of Mg-doping, θ_p is also negative but very small, and antiferromagnetic coupling between local moments is negligible. Although Mg atoms or ions are not a magnetic element, the electrons doped into B framework may produce local moments. The spin density, N , in Eq. (4) should be proportional to the dopant concentration. Fig. 9 shows the relation between the dopant content at each site and C . Obviously, only the content of Mg at D site showed a linear correlation with C . Thus, the dopants other than Mg at the D site are not causing the observed CW component. Another possibility is the impurity contained not only in B but also in Mg used for the VDP, which may be introduced into the samples together with Mg, because the CW

Table 4

Temperature-independent magnetic susceptibility, χ_0 , Currie constant, C , and Currie temperature, θ_p , for the selected samples obtained by a fitting of Eq. (3) to the experimental results

Sample name	χ_0 (10^{-7} emu/gOe)	C (10^{-5} emu/gOe K)	θ_p (K)
β -B (2 N)	-9.2	6.7	-8.3
Mg- β -1	-9.6	6.2	-3.3
Mg- β -2	-9.2	8.3	-3.1
Mg- β -3	-8.4	10	-3.5
Mg- β -6	-7.3	9.3	-3.4
Mg- β -8	-6.4	9.1	-3.6
Mg- β -10	-6.8	5.8	-3.1

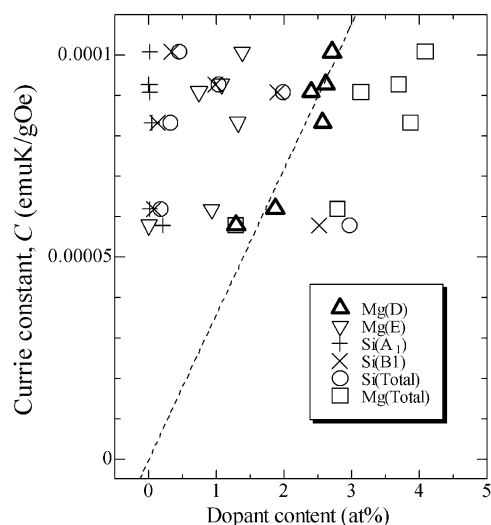


Fig. 9. Relation between Currie constant and the dopant content. Dashed line crossing the origin shows the linearity of the Currie constant on the dopant content for Mg at D site.

component increased after the Mg-doping. According to the report of the supplier, the used Mg metal contains 0.01 Zn, 0.007 Si, 0.007 Al, 0.004 Fe, 0.004 Mn, 0.001 Cu and 0.001 Ni in wt%. Among them, most effective element for ferromagnetism is Fe. We examined the content of the Fe in Mg- β -6 and 10 by using an inductively coupled plasma (ICP) measurement. The content was 0.03 wt% for both. Assuming that the p_{eff} of Fe^{3+} and Fe^{2+} are 5.8 and 5.2, respectively, we calculated the corresponding content of Fe with the values of C . The resulting values ranged between 0.1 and 0.2 wt%, which are much larger than the content obtained by the ICP. Also, the value of C for Mg- β -6 is almost double of that for Mg- β -10 although the content measured by ICP was same for the both. Thus, the amounts of the impurities from the Mg source are too small to explain the appearance of the CW component.

The temperature-independent part, χ_0 , contains diamagnetism because the χ is negative even at room

temperature. χ_0 can be written as

$$\chi_0 = \chi_p + \chi_L + \chi_d, \quad (5)$$

where χ_p is due to the Pauli paramagnetism, χ_L the Landau diamagnetism and χ_d the closed-shell diamagnetism including Larmor diamagnetism. Among them, the χ_d is not supposed to be affected by doping of metals. Accordingly, one can express $\Delta\chi_0$, which is the change of the χ_0 due to the doping, as

$$\Delta\chi_0 = \Delta\chi_p + \Delta\chi_L = \frac{2}{3} \mu_B^2 \Delta N(E_F), \quad (6)$$

where $\Delta N(E_F)$ is the difference of the $N(E_F)$ from that of the undoped sample. Therefore, the dependence of $\Delta\chi_0$ on the dopant content corresponds to that of $\Delta N(E_F)$. The $\Delta N(E_F)$ can be approximately taken as $N(E_F)$ because the undoped β -B is semiconductor, whose $N(E_F)$ is nearly zero. As described in the introduction, the number of electrons donated by the dopants has important meaning for the metal transition of doped β -B because we can expect that the donated electrons fill up the IAL and Fermi energy will reach to the conduction band. The capacity of IAL is 8 electrons/ B_{105} . By assuming that each Mg atom donates 2 electrons and the Si atom doped at B1 by replacing a B atom donates one electron, we can calculate the number of doped electrons from their site occupancies. Fig. 10 shows the relation between the $\Delta N(E_F)$ and the number of doped electrons. The $\Delta N(E_F)$ increases at the total number of electrons more than 8. The sample names indicated in the figure with arrows correspond to those used for the EELS measurement. As discussed above, the appearance of Fermi edge indicated the metal transition only for the samples Mg- β -3 and 8. The total number of electrons for Mg- β -1 (6.2) is less than 8. On the other hand, the numbers for Mg- β -3 and 8 are 8.9 and 8.6, respectively. The number of doped electrons for Mg- β -8 only from the Mg atoms is 6.6, which is less than 8 although both of the results of the EELS measurement and the $\Delta N(E_F)$ show that metal transition occurred for the sample. Thus, we conclude that more than 8

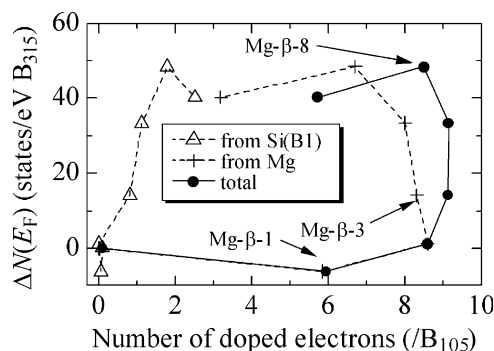


Fig. 10. Relation between number of doped electrons and the $\Delta N(E_F)$ calculated from the results of magnetic susceptibility measurement.

electrons donated both from the Si atoms at the B1 site and Mg atoms pushed the Fermi energy above the IAL and caused metal transition.

4. Conclusion

Li and Mg were doped into α -B only partially by the VDP. About 0.02 vol% of a superconductive phase with T_C of 36 K was found in only one of the Li-doped α -B samples by the measurement of the temperature dependence of the magnetic susceptibility. Mg was doped into β -B homogeneously by the VDP method up to 4 at% ($\text{Mg}_{4.1}\text{B}_{105}$), although a considerable amount of Si was co-doped into the sample. The Mg is doped at the *D*, *E* and *F* interstitial sites and the Si is doped at the A_1 interstitial and B1 substitutional site. The expansions of the lattice are substantially due to the Mg-doping for the *c*-axis direction and the Si-doping for the *a*-axis direction. A temperature-dependent component of the magnetic susceptibility, which obeys the Curie–Weiss law, was observed and the intensity of the component was proportional to the content of the doped Mg at *D* site, although the origin of the magnetism is not clear. Although superconductivity was not observed for the Mg-doped β -B, the results of the measurement of the EELS and the magnetic susceptibility suggest a metal transition of the β -B by the doping of more than 8 electrons/ B_{105} , which are donated from the doped Mg and Si. This fact implies that the doped electrons filled up the IAL with capacity of 8 electrons and the Fermi energy reached the conduction band in the rigid band scheme of the β -B.

Acknowledgments

The authors thank Prof. I. Higashi (Chiba Institute of Technology) for valuable advices on the structural analysis, Prof. H. Suematsu (University of Tokyo) and Mr. S. Sato (Cryogenic Center, University of Tokyo) for support of magnetic measurements using SQUID. This research was supported by the Mitsubishi Foundation and a Grants-in-Aid for Scientific Research from Japan Society for the Promotion of Science (JSPS).

References

- [1] M. Vlasse, J.C. Viala, *J. Solid State Chem.* 37 (1981) 181–188.
- [2] B. Callmer, T. Lundström, *J. Solid State Chem.* 17 (1976) 165–170.

- [3] M.F. Garbaskas, J.S. Kasper, G.A. Slack, *J. Solid State Chem.* 63 (1986) 424–430.
- [4] M. Kobayashi, I. Higashi, H. Matsuda, K. Kimura, *J. Alloys Compd.* 221 (1995) 120–124.
- [5] H.K. Clark, *J. Am. Chem. Soc.* 65 (1943) 2115–2119.
- [6] E. Amberger, P.A. Rauh, *Acta Crystallogr. B* 30 (1974) 2549–2553.
- [7] I. Higashi, M. Kobayashi, J. Bernhard, C. Brodhag, F. Thevenot, *AIP Conf. Proc.* 231 (1991) 201–204.
- [8] H. Matsuda, T. Nakayama, K. Kimura, Y. Murakami, H. Suematsu, I. Higashi, M. Kobayashi, *Phys. Rev. B* 52 (1995) 6102–6110.
- [9] H. Matsuda, N. Tanaka, T. Nakayama, K. Kimura, Y. Murakami, H. Suematsu, M. Kobayashi, I. Higashi, *J. Phys. Chem. Solids* 57 (1996) 1167–1174.
- [10] T. Nakayama, H. Matsuda, K. Kimura, H. Ino, *J. Solid State Chem.* 133 (1997) 342–346.
- [11] T. Nakayama, J. Shimizu, K. Kimura, *J. Solid State Chem.* 154 (2000) 13–19.
- [12] H. Yamaguchi, Y. Sakairi, M. Takeda, K. Kimura, E. Matsu- bara, *Trans. Mater. Res. Soc. Jpn.* 24 (1999) 85–88.
- [13] M. Takeda, M. Ichimura, H. Yamaguchi, Y. Sakairi, K. Kimura, *J. Solid State Chem.* 154 (2000) 141–144.
- [14] S. Gunji, H. Kamimura, T. Nakayama, *J. Phys. Soc. Jpn.* 62 (1993) 2408–2418.
- [15] S. Gunji, H. Kamimura, *Phys. Rev. B* 54 (1996) 13665–13673.
- [16] M.C. Böhm, J. Schulte, R. Schlögl, *Phys. Stat. Sol.* 196 (1996) 131–144.
- [17] A. Oshiyama, S. Saito, N. Hamada, Y. Miyamoto, *J. Phys. Chem. Solids* 53 (1992) 1457–1471.
- [18] M.Z. Huang, Y.N. Xu, W.Y. Ching, *Phys. Rev. B* 46 (1992) 6572–6577.
- [19] J. Nagamatsu, N. Nakagawa, T. Muranaka, Y. Zenitani, J. Akimitsu, *Nature* 40 (2001) 63–64.
- [20] J.M. An, W.E. Pickett, *Phys. Rev. Lett.* 86 (2001) 4366–4369.
- [21] H.J. Choi, D. Roundy, H. Sun, M.L. Cohen, S.G. Loule, *Nature* 418 (2002) 758–760.
- [22] C. Wood, D. Emin, *Phys. Rev. B* 29 (1984) 4582–4587.
- [23] J.A. Ugai, N.E. Soloviev, in: V.I. Matkovich (Ed.), *Boron and Refractory Borides*, Springer, New York, 1977, p. 227.
- [24] M. Terauchi, Y. Kawamata, M. Tanaka, M. Takeda, K. Kimura, *J. Solid State Chem.* 133 (1997) 156–159.
- [25] F. Izumi, T. Ikeda, *Mater. Sci. Forum* 321–323 (2000) 198–203.
- [26] M. Terauchi, A. Oguri, K. Kimura, *Phys. Rev. Lett.*, submitted for publication.
- [27] M. Terauchi, Y. Sato, A. Oguri, K. Soga, T. Nakayama, K. Kimura, *J. Solid State Chem.*, submitted for publication.
- [28] A. Oguri, K. Kimura, A. Fujiwara, M. Terauchi, M. Tanaka, *AIP Conf. Proc.* 590 (2001) 507–510.
- [29] S. Bruttì, M. Colapietro, G. Balducci, L. Barba, P. Manfrinetti, A. Palenzona, *Intermetallics* 10 (2002) 811–817.
- [30] G.A. Slack, C.I. Hejna, M.F. Garbaskas, J.S. Kasper, *J. Solid State Chem.* 76 (1988) 52–63.
- [31] J.I. Langford, D. Louer, *Rep. Progr. Phys.* 59 (1996) 131–234.
- [32] G.P. Tsiskarisvili, T. Lundstrom, L. Lundgren, G.V. Tsagar- eishvili, D.N. Tsikardze, F.N. Tavazde, *J. Less-Common Metals* 147 (1989) 41–49.
- [33] G.P. Tsiskarisvili, T. Lundstrom, L. Lundgren, G.V. Tsagar- eishvili, O.A. Tsagareishvili, F.N. Tavazde, *J. Less-Common Metals* 142 (1988) 91–104.